Journal of the Ceramic Society of Japan 124 [1] 1-6 2016 Full paper

Mechanical strength and electrical conductivity of reactively-sintered pseudobrookite-type Al_2TiO_5–$MgTi_2O_5$ solid solutions

Ryosuke S. S. MAKI[*] and Yoshikazu SUZUKI[*,,†]**

[*]**Graduate School of Pure and Applied Sciences, University of Tsukuba, 1–1–1 Tennodai, Ibaraki 305–8573, Japan**
[**]**Faculty of Pure and Applied Sciences, University of Tsukuba, 1–1–1 Tennodai, Ibaraki 305–8573, Japan**

Al_2TiO_5–$MgTi_2O_5$ solid solutions were synthesized by reactive sintering of α-Al_2O_3, TiO_2 anatase and $MgCO_3$ (basic) powders at 1400°C (and at 1300°C for some composition) for 2 h, with changing the $MgTi_2O_5$ ratio to form the composition of $Al_{2(1-x)}Ti_{1+x}Mg_xO_5$ ($x = 0.0$–1.0) and evaluated their properties. With increasing $MgTi_2O_5$ molar ratio, the matrix Al_2TiO_5–$MgTi_2O_5$ grains became more anisotropic, and the coefficient of thermal expansion increased due to the decrease of microcracks. $Al_{0.2}Ti_{1.9}Mg_{0.9}O_5$ ($x = 0.9$) showed the maximum strength of 47.9 MPa. On the other hand, $MgTi_2O_5$ ($x = 1.0$) showed low bending strength of 13.2 MPa due to the grain growth during the sintering at 1400°C. $Al_{0.6}Ti_{1.7}Mg_{0.7}O_5$ ($x = 0.7$) sintered at 1300°C indicated the highest conductivity. The conductivity of pseudobrookite-type ceramics strongly depends on microcracks.

Key-words : Reactive sintering, Mechanical properties, Electrical conductivity, Thermal expansion, Al_2TiO_5, $MgTi_2O_5$

[Received April 16, 2015; Accepted May 22, 2015]

1. Introduction

Al_2TiO_5 with pseudobrookite-type structure has been widely studied because of (a) its low coefficients of thermal expansion (CTE), (b) its high melting point and (c) its high thermal shock resistance.[1)] Since low thermal expansion materials are necessary under some specific high-temperature applications, such as a thermistor and a heat exchanger, pseudobrookite-type ceramics are widely used for these devices.[2)] The low CTE of Al_2TiO_5, however, is attributed to microcracks caused by anisotropic thermal expansion under cooling from the sintering temperature. Therefore, sintered Al_2TiO_5, usually not fully dense, generally shows low fracture strength.[3)]

Bayer[4)] reported that the CTE of pseudobrookite-type Al_2TiO_5 for each crystalline axis (space grope: *Cmcm*) were $\beta_a = -3.0 \pm 0.3$, $\beta_b = 11.8 \pm 0.6$, $\beta_c = 21.8 \pm 1.1$ ($\times 10^{-6}$/°C) in a temperature range of 20–1020°C. The CTE of polycrystalline Al_2TiO_5 ceramics, however, was rather small as an oxide, typically reported as $<2.0 \times 10^{-6}$/°C.[5),6)] Despite the fascinating low thermal expansion behavior, Al_2TiO_5 is not so thermally stable and decomposes into Al_2O_3 and TiO_2 below the equilibrium temperature of 1280°C,[7)] which limits the applications of Al_2TiO_5, particularly in reducing atmosphere.

Besides Al_2TiO_5, several ceramics with pseudobrookite-type structure, such as $MgTi_2O_5$ and Fe_2TiO_5 were investigated.[4)] Solid solutions of pseudobrookite-type structure (e.g. $Al_{2(1-x)}Fe_{2x}TiO_5$[8)] and others[9),10)]) have also been synthesized and their CTE, thermal stabilities and microstructures have been reported.[11)] $MgTi_2O_5$ with pseudobrookite-type structure has potentially good mechanical properties with high thermal shock resistance, because its thermal expansion anisotropy is smaller than Al_2TiO_5.[12)–15)] To date, $MgTi_2O_5$ has been investigated for a third-generation diesel particulate filter with low cost, high temperature stability and better mechanical properties than Al_2TiO_5.[16)–18)] $MgTi_2O_5$ can be synthesized in an intermediate temperature range of 1000–1200°C because of relatively high temperature stability among pseudobrookite-type ceramics. $MgTi_2O_5$ stabilizes the crystal phase of Al_2TiO_5 by forming an all-proportional solid solution. Therefore $MgTi_2O_5$ has been used as a stabilizer of Al_2TiO_5 in order to restrain the decomposition of Al_2TiO_5 in a temperature range of 750–1300°C (decomposition temperature of $MgTi_2O_5$ is 130–230°C[19)]). For these reasons, Al_2TiO_5–$MgTi_2O_5$ solid solution with intermediate feature between Al_2TiO_5 and $MgTi_2O_5$ has been studied as low CTE material with relatively high fracture strength.[15),20),21)]

As for Al_2TiO_5–$MgTi_2O_5$ solid solutions, there have been several studies on CTE and microstructures. However, relatively few studies have been reported on the functional properties of pseudobrookite-type ceramics, such as dielectric properties,[22)–25)] photocatalytic function[26),27)] and electrical properties.[28),29)]

In this study, we have synthesized Al_2TiO_5–$MgTi_2O_5$ solid solutions from α-Al_2O_3, TiO_2 anatase and $MgCO_3$ (basic) powders by reactive sintering method, with changing the $MgTi_2O_5$ ratio to form the composition of $Al_{2(1-x)}Ti_{1+x}Mg_xO_5$ ($x = 0.0$–1.0) and evaluated their properties. First, CTE and fracture strength of Al_2TiO_5–$MgTi_2O_5$ solid solutions (7 compositions including end members) were systematically characterized. Second, electrical conductivity of these Al_2TiO_5–$MgTi_2O_5$ solid solutions were also systematically measured by AC impedance method. For the pseudobrookite-type $Mg_xTi_{3-x}O_5$ ($x = 0.2$, 0.3, 0.5, 0.8 and 0.9), a systematic analysis of electrical conductivity at 800°C was carried out by Steiner et al.[28)] However, such a systematic analysis on the Al_2TiO_5–$MgTi_2O_5$ solid solutions has not yet been reported. Temperature dependence of electrical properties was discussed for a solid solution with the highest conductivity.

† Corresponding author: Y. Suzuki; E-mail: suzuki@ims.tsukuba.ac.jp
‡ Preface for this article: DOI http://dx.doi.org/10.2109/jcersj2.124.P1-1

DOI http://dx.doi.org/10.2109/jcersj2.15098

2. Experimental

2.1 Sample preparation

Commercial α-Al_2O_3 (99.99% purity, Taimei Chemicals Co. Ltd., Saitama, Japan), TiO_2 anatase (99% purity, Kojundo Chemical Laboratory Co. Ltd.) and $MgCO_3$ (basic) [99.9% purity, Kojundo Chemical Laboratory Co. Ltd., with actual composition of $Mg_5(CO_3)_4(OH)_2{\cdot}4H_2O$] powders were used as starting materials. $MgCO_3$ (basic) includes hydroxyl groups and hydrated water. Hence, prior to the powder mixing, each starting powder was characterized by thermogravimetry-differential thermal analysis (TG–DTA) to clarify the weight-loss during the heating up to 1000°C. Required powder weight was corrected using the TG–DTA results. α-Al_2O_3, TiO_2 anatase and $MgCO_3$ (basic) powders were weighed according to the final compositions of Al_2TiO_5–$MgTi_2O_5$ solid solutions, expressed as $Al_{2(1-x)}Ti_{1+x}Mg_xO_5$, where x is the molar ratio of $MgTi_2O_5$. The powders were mixed by wet ball-milling with ZrO_2 media for 2 h using ethanol. The slurries were dried in an evaporator, and then, dried at 80°C in air. The dried powders were dry ball-milled with ZrO_2 balls for 2 h, and were sieved through a 150-mesh screen. Cylindrical pellets (diameter of 15 mm) and rectangular bars (4 × 6 × 50 mm) were prepared by the uniaxial press of mixed powders. The green samples were obtained by cold isostatic pressing (CIP) at 200 MPa for 10 min. Subsequently, the green samples were sintered at 1400°C (or 1300°C for some samples) for 2 h in air to obtain dense samples.

2.2 Phases and microstructure

Constituent phases of sintered Al_2TiO_5–$MgTi_2O_5$ solid solution samples were analyzed by X-ray powder diffraction (Multiflex, Cu-Kα, 40 kV and 40 mA, Rigaku, Japan). Prior to the powder XRD measurement, the sintered samples were pulverized with an agate mortar using ethanol, and the XRD patterns were collected in the range of $2\theta = 10$–$70°$. ICDD-JCPDS database was used for identifying constitution phase and indexing pseudobrookite phase.

Microstructure of the samples was observed by scanning electron microscopy (TM3000 Table Microscope, Hitachi, Japan). The samples were coated with Au by sputtering (SC-701, 3.5 mA for 5 min, Sanyu Electron, Japan). In order to evaluate the size of microcracks, mirror surfaces polished with 9, 3 and 0.5 µm diamond slurries were observed. Energy dispersive X-ray spectrometry (EDS) was carried out for an elemental analysis of surface of the sintered samples. For EDS analysis, un-coated samples were used not to detect Au peaks.

2.3 Density and mechanical properties

The bulk densities of the sintered samples were measured by mass and dimensions. For CTE measurement, the sintered rectangular bars were machined into the test pieces (the length of measured direction is 10–20 mm) with waterproof abrasive papers. The CTE was evaluated by thermomechanical analysis (Thermo plus EVO II, RIGAKU, Japan) in a temperature range of 50–1000°C.

In order to evaluate fracture strength, sintered rectangular bars were machined into the test specimens. The tensile face and corners of each specimen were polished and chamfered by waterproof abrasive paper. Fracture strength was measured by three-point bending test with a span of 30 mm and crosshead speed of 0.5 mm/min by using a universal testing machine (Autograph AG-20kN, Shimadzu Co. Ltd., Japan). Three to five specimens were used for each measurement.

2.4 Electrical properties

The surfaces of the sintered pellets were polished by waterproof abrasive paper to enhance electrode adhesion. Platinum paste electrodes and platinum wires were attached to the surfaces of sintered pellets and heated up to 1200°C for 1 h. The pellet was positioned in the center of a tubular furnace. Impedance spectra were measured at 750–1000°C in air over the frequency range of 5 Hz to 13 MHz. A K-type thermocouple was placed in the tubular furnace to monitor the temperature vicinity to the pellet. Prior to the impedance measurement, the temperature was kept at the target temperature for 20 min to stabilize the sample temperature.

3. Results and discussion

3.1 Phases and microstructure

Figure 1 shows XRD patterns of the samples with the composition of $Al_{2(1-x)}Ti_{1+x}Mg_xO_5$ ($x = 0.1$–1.0), where x is the molar ratio of $MgTi_2O_5$, obtained by reactive sintering at 1400°C for 2 h. By using the calibrated starting powder, XRD data of all samples sintered at 1400°C represented single Al_2TiO_5–$MgTi_2O_5$ solid solution [pseudobrookite-type phase, space group: *Cmcm*(63)]. The $Al_{2(1-x)}Ti_{1+x}Mg_xO_5$ ($x = 1.0$, i.e. $MgTi_2O_5$) sample was composed of only pseudobrookite-type phase. The $Al_{2(1-x)}Ti_{1+x}Mg_xO_5$ ($x = 0.0$, i.e. Al_2TiO_5) sample was composed mainly of pseudobrookite-type phase with trace of Al_2O_3 and TiO_2 phase. The easier formation of pseudobrookite-type $MgTi_2O_5$ (formable at 920°C[4]) can be attributed to the smaller size-difference between Mg^{2+} ion and Ti^{4+} ion than the size-difference between Al^{3+} ion and Ti^{4+} ion. The $Al_{1.8}Ti_{1.1}Mg_{0.1}O_5$ ($x = 0.1$) sample, despite low molar ratio of $MgTi_2O_5$, was composed of only pseudobrookite-type phase, because of the decrease in distortion of MO_6 octahedra, due to the substitution of metal ions ($2Al^{3+} \Leftrightarrow Mg^{2+} + Ti^{4+}$).[15]

Figure 2 exhibits typical SEM images of the surfaces of $Al_{2(1-x)}Ti_{1+x}Mg_xO_5$ ($x = 0.1$, 0.3, 0.7 and 1.0) samples with Au coating. The increases of grain size and densifications with increasing $MgTi_2O_5$ molar ratio were confirmed. With increasing $MgTi_2O_5$ molar ratio, the matrix Al_2TiO_5–$MgTi_2O_5$ grains became more anisotropic. The grain size and anisotropy depended on the molar ratio of Al_2TiO_5: $MgTi_2O_5$. $MgTi_2O_5$ ($x = 1.0$) sample consisted of relatively dense matrix with larger grains (~10–50 µm in length). These results can be attributed to the linear decrease of formation temperature of pseudobrookite-type phase, as reported by Daimon.[15] By the decrease of formation

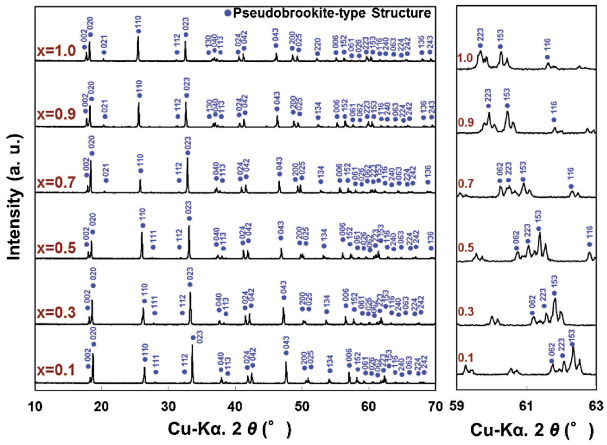

Fig. 1. XRD patterns of $Al_{2(1-x)}Ti_{1+x}Mg_xO_5$ ($x = 0.0$–1.0) solid solutions sintered at 1400°C for 2 h. [ICDD-JCPDS35-0792 ($x = 1.0$), ICDD-JCPDS 34-1062 ($x = 0.6$), ICDD-JCPDS 33-0854 ($x = 0.3$)].

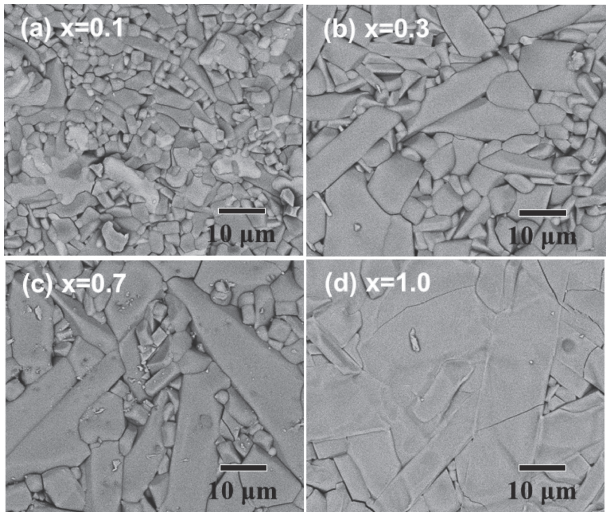

Fig. 2. Microstructure of $Al_{2(1-x)}Ti_{1+x}Mg_xO_5$ ($x = 0.0$–1.0) solid solutions sintered at 1400°C for 2 h: (a) $x = 0.1$, (b) $x = 0.3$, (c) $x = 0.7$ and (d) $x = 1.0$.

Table 1. Elemental Analysis of Surface of $Al_{2(1-x)}Ti_{1+x}Mg_xO_5$ ($x = 0.1$–1.0) Solid Solutions

$Al_{2(1-x)}Ti_{1+x}Mg_xO_5$	Atomic (%)			
	Al	Mg	Ti	O
$x = 0.1$	20.7	1.3	14.5	63.5
$x = 0.3$	14.5	3.2	13.5	68.8
$x = 0.7$	5.9	7.6	18.2	68.3
$x = 0.9$	1.5	10.2	19.7	68.6
$x = 1.0$	—	11.7	22.1	66.2

temperature, pseudobrookite-type structure became more stable for solid-solutions, resulting more rapid and more anisotropic grain growth with increasing $MgTi_2O_5$ content.

EDS elemental analysis was carried out on the surface of uncoated samples. **Table 1** summarizes atomic percent of $Al_{2(1-x)}Ti_{1+x}Mg_xO_5$ ($x = 0.1$–1.0) samples. Target composition and measured composition by EDS analysis were in good agreement with each other. In a specific composition (e.g., $x = 0.3$), some large and small grains were analyzed by EDS point analysis, however, there were almost no compositional difference.

3.2 Density and mechanical properties

Figure 3 shows relative density as a function of composition [$Al_{2(1-x)}Ti_{1+x}Mg_xO_5$ ($x = 0.0$–1.0)] obtained by reactive sintering at 1400°C for 2 h. The relative densities of $Al_{2(1-x)}Ti_{1+x}Mg_xO_5$ ($x = 0.1$–1.0) were much higher than that of $Al_{2(1-x)}Ti_{1+x}Mg_xO_5$ ($x = 0.0$). $Al_{0.2}Ti_{1.9}Mg_{0.9}O_5$ ($x = 0.9$) sintered at 1400°C showed the highest relative density, 92.6%.

Figure 4 represents CTE as a function of composition [$Al_{2(1-x)}Ti_{1+x}Mg_xO_5$ ($x = 0.0$–1.0)]. $Al_{2(1-x)}Ti_{1+x}Mg_xO_5$ ($x = 0.1$–0.3) exhibits relatively low thermal expansion values and $Al_{2(1-x)}Ti_{1+x}Mg_xO_5$ ($x = 0.0$–0.1) showed negative thermal expansion behavior up to 950°C. Thermal expansion increased with increasing $MgTi_2O_5$ ratio due to decrease of microcracks. $Al_{2(1-x)}Ti_{1+x}Mg_xO_5$ ($x = 0.0$), however, did not represent the lowest thermal expansion. In our previous work,[30] we revealed that secondary phase dispersion is effective to reduce the Al_2TiO_5 matrix grain size and to reduce the strong anisotropy of Al_2TiO_5, which resulted in fewer microcracks. In the XRD result, $Al_{2(1-x)}Ti_{1+x}Mg_xO_5$ ($x = 0.0$) was mainly composed of pseudobrookite-type phase with some Al_2O_3 and TiO_2 phases. Therefore, co-existed Al_2O_3 and TiO_2 grains probably inhibited the anisotropic grain growth of Al_2TiO_5.

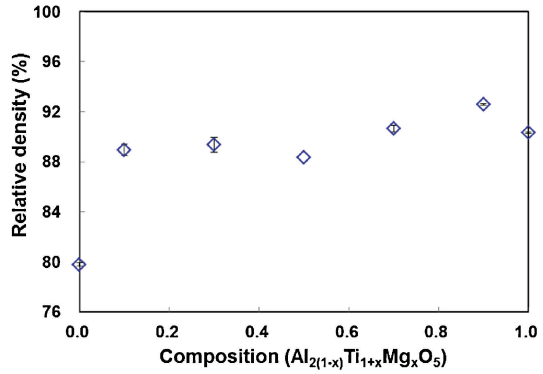

Fig. 3. Relative density of $Al_{2(1-x)}Ti_{1+x}Mg_xO_5$ ($x = 0.0$–1.0) solid solutions sintered at 1400°C for 2 h. The full density of each composition was calculated by the Vegard's law.

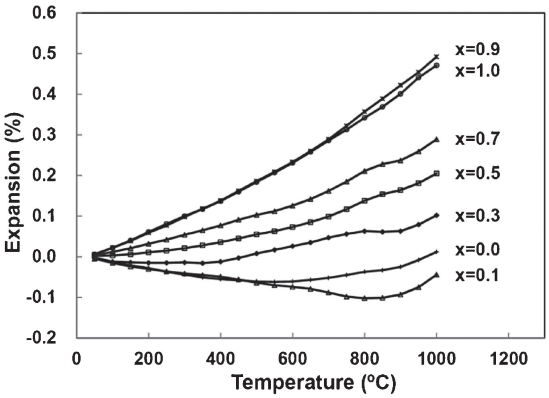

Fig. 4. Thermal expansion coefficients of $Al_{2(1-x)}Ti_{1+x}Mg_xO_5$ ($x = 0.0$–1.0) solid solutions sintered at 1400°C for 2 h.

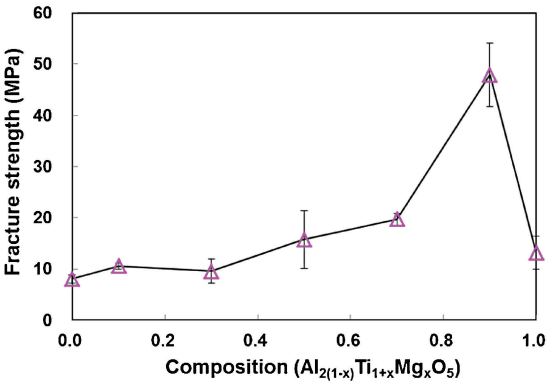

Fig. 5. Fracture strengths of $Al_{2(1-x)}Ti_{1+x}Mg_xO_5$ ($x = 0.0$–1.0) solid solutions sintered at 1400°C for 2 h. $x = 0.9$ shows the highest fracture strength, 47.93 MPa.

Figure 5 shows bending strength as a function of composition [$Al_{2(1-x)}Ti_{1+x}Mg_xO_5$ ($x = 0.0$–1.0)]. $Al_{2(1-x)}Ti_{1+x}Mg_xO_5$ ($x = 0.0$) indicated 8.1 MPa. Bending strength of $Al_{2(1-x)}Ti_{1+x}Mg_xO_5$ ($x = 0.0$–0.9) increased with increasing $MgTi_2O_5$ ratio due to the decrease of microcracks. $Al_{0.2}Ti_{1.9}Mg_{0.9}O_5$ ($x = 0.9$) showed the maximum strength of 47.9 MPa. On the other hand, $MgTi_2O_5$

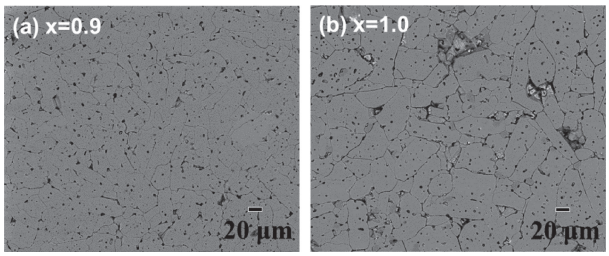

Fig. 6. Microstructure of $Al_{2(1-x)}Ti_{1+x}Mg_xO_5$ ($x = 0.9$, 1.0) solid solutions sintered at 1400°C for 2 h: (a) $x = 0.9$ and (b) $x = 1.0$.

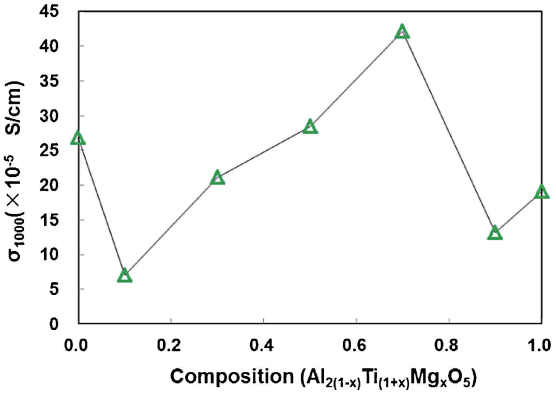

Fig. 7. Conductivity of $Al_{2(1-x)}Ti_{1+x}Mg_xO_5$ ($x = 0.0$–1.0) solid solutions sintered at 1400°C for 2 h. $x = 0.7$ showed the highest conductivity, 42.12×10^{-5} S/cm.

($x = 1.0$) showed very low bending strength of 13.2 MPa due to the grain growth during the sintering at 1400°C, despite its high relative density and high CTE. The low strength of $MgTi_2O_5$ is attributable to the crack growth accompanied by the grain growth, as shown in **Fig. 6**, which shows mirror surfaces of $Al_{2(1-x)}Ti_{1+x}Mg_xO_5$ ($x = 0.9$, 1.0) solid solutions sintered at 1400°C.

3.3 Electrical properties

Figure 7 shows the electrical conductivity as a function of composition [$Al_{2(1-x)}Ti_{1+x}Mg_xO_5$ ($x = 0.0$–1.0)] at 1000°C in air. In this work, $Al_{1.8}Ti_{1.1}Mg_{0.1}O_5$ ($x = 0.1$) indicated the lowest conductivity, and $Al_{0.6}Ti_{1.7}Mg_{0.7}O_5$ ($x = 0.7$) indicated the highest conductivity. This complicated conductivity dependence is attributable to (1) grain size, (2) secondary phases ($x = 0$, i.e. Al_2O_3 and TiO_2 dispersion), (3) large microcracks for $x = 0.9$ and 1.0, and (4) density change (Fig. 3).

Since the composition of $Al_{0.6}Ti_{1.7}Mg_{0.7}O_5$ ($x = 0.7$) showed the highest conductivity, we focused on this composition in the following part. In order to examine the effect of sintering temperature on the conductivity, the sample was also sintered at 1300°C as well as 1400°C. By lowering the sintering temperature (from 1400 to 1300°C), the sample had smaller grain size and hence smaller microcracks, as well as somewhat smaller density.

Figure 8 shows typical surface SEM images of $Al_{0.6}Ti_{1.7}Mg_{0.7}O_5$ ($x = 0.7$) samples sintered at (a) 1400°C and (b) 1300°C. XRD (not shown) confirmed that the $Al_{0.6}Ti_{1.7}Mg_{0.7}O_5$ ($x = 0.7$) sample sintered at 1300°C was also composed of single pseudobrookite-type phase. The sample sintered at 1300°C had a bi-modal structure, i.e., anisotropic large grains and anisotropic small grains (shown in the inset). The relative density of $Al_{2(1-x)}Ti_{1+x}Mg_xO_5$ ($x = 0.7$) samples sintered at (a) 1400°C and (b) 1300°C were 90.7 and 88.6%, respectively.

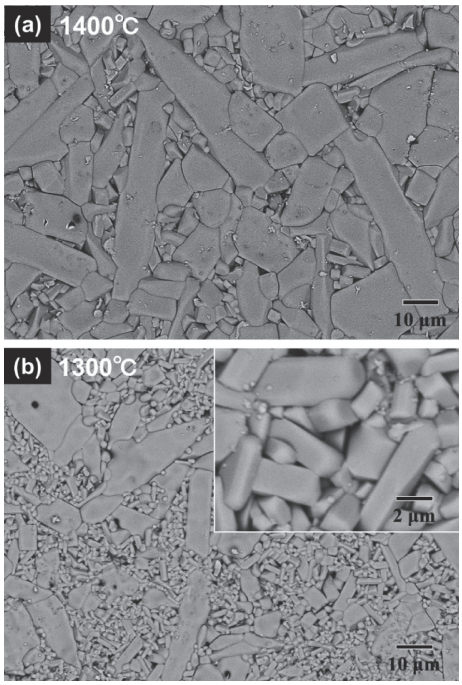

Fig. 8. Microstructure of $Al_{0.6}Ti_{1.7}Mg_{0.7}O_5$ solid solutions sintered at (a) 1400°C and (b) 1300°C.

Figure 9 represents Cole–Cole plots of $Al_{0.6}Ti_{1.7}Mg_{0.7}O_5$ ($x = 0.7$) sintered at (a) 1400°C and (b) 1300°C, measured over the frequency range 5 Hz to 13 MHz at temperature between 750–900°C in air. Two semicircular arcs, one with high frequency and another with low frequency, can be observed. The one with high frequency and the other one with low frequency corresponds to grain and grain boundary, respectively. The total resistivity of the sample sintered at 1400°C was higher than that of sintered at 1300°C at each measuring temperature, and each semicircular arc (grain and grain boundary) showed decrease in resistivity with increasing measuring temperature. The grain-boundary resistivity of the sample sintered at 1400°C was higher in spite of less grain boundaries than that of sample sintered at 1300°C.

The results in Fig. 9 suggest that conductivity of pseudobrookite-type ceramics strongly depends on microcracks. Several researchers reported that microcracks show crack healing at high temperature.[31),32)] The decrease of grain-boundary resistivity at high measuring temperatures is attributed to microcrack-healing behavior. For example, the grain boundary resistivity of the sample sintered at 1300°C had little effect on total resistivity at 900°C [see the insert of Fig. 9(b)]. The reason of small grain-boundary resistivity at 900°C can be explained as follows. According to the Bayer's report,[4)] the average CTE (20–1020°C) of Al_2TiO_5 single crystal and $MgTi_2O_5$ single crystal were calculated as 10.2×10^{-6} and 9.67×10^{-6}/K, respectively. While in this study, the measured CTE at 900–1000°C of the samples sintered at 1400 and 1300°C were 5.23×10^{-6} and 8.90×10^{-6}/K, respectively. The value of 5.23×10^{-6}/K for the sample sintered at 1400°C is clearly smaller than that of the calculated values of $\sim 10 \times 10^{-6}$/K and that of the sample sintered at 1300°C. Thus, the sample sintered at 1400°C still contained open microcracks at 900°C, while a plenty of microcracks of the sample sintered at 1300°C seem to be closed at 900°C.

Arrhenius plots of the conductivity and electrical properties of $Al_{0.6}Ti_{1.7}Mg_{0.7}O_5$ ($x = 0.7$) sintered at (a) 1400°C and (b)

Table 2. Electrical properties of $Al_{0.6}Ti_{1.7}Mg_{0.7}O_5$ solid solutions sintered at 1400 and 1300°C

Sintering temperature (°C)	Relative density (%)	Conductivity		E_a(eV)	
		$\sigma_{1000}(\times10^{-5}$ S/cm)	$\sigma_{900}(\times10^{-5}$ S/cm)	G	GB
1400	90.7	42.1	8.9	3.9	4.9
1300	88.6	46.5	10.3	3.6	4.5

E_a: activation energy (G: grain, GB: grain boundary).

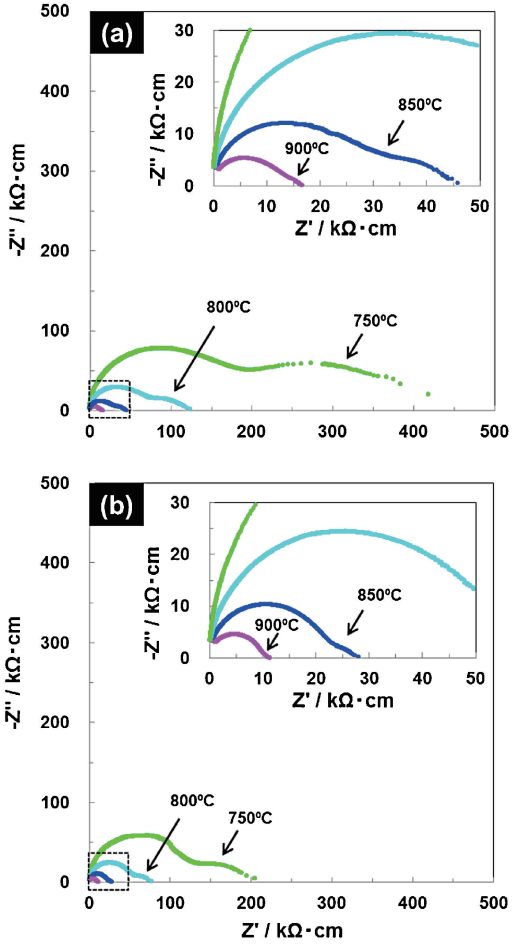

Fig. 9. Cole–Cole plots of $Al_{0.6}Ti_{1.7}Mg_{0.7}O_5$ solid solutions sintered at (a) 1400°C and (b) 1300°C measured in the temperature range of 750–900°C in air. Impedance plots measured at 850–900°C are shown in the insets.

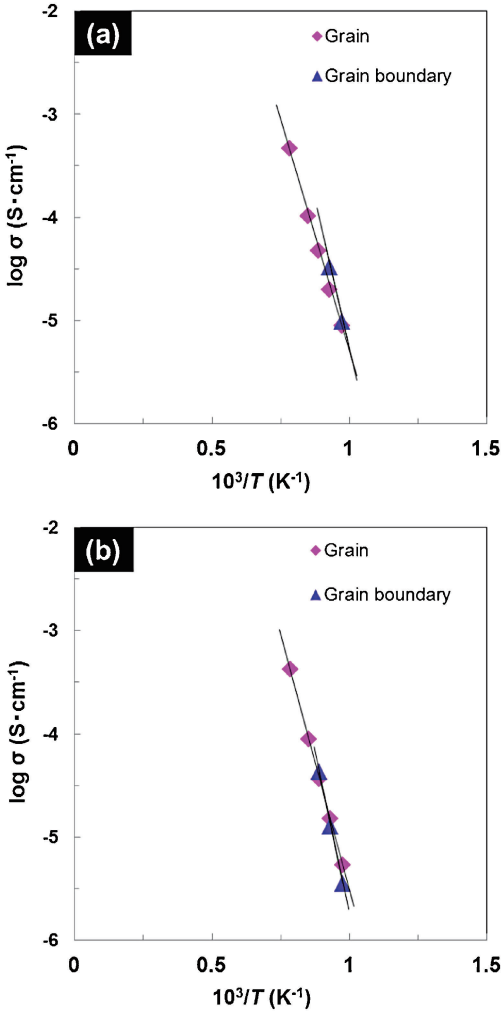

Fig. 10. Arrhenius plots of the conductivity of $Al_{0.6}Ti_{1.7}Mg_{0.7}O_5$ solid solutions sintered at (a) 1400°C and (b) 1300°C.

1300°C are shown in **Fig. 10** and **Table 2**. The activation energy (eV) in grain of samples sintered at 1400 and 1300°C were 3.9 and 3.6, respectively, while the activation energy in grain boundary of samples sintered at 1400 and 1300°C were 4.9 and 4.5, respectively. The sample sintered at 1400°C hence showed somewhat stronger temperature dependence than that at 1300°C. This result also suggested the increase of the amount of microcracks with increasing sintering temperature. In this study, the activation energy in grain boundary was higher than that in grain. Since the microcracks were mainly formed at grain boundaries, temperature dependence of the conductivity became more sensitive at grain boundary than in grain. These results are in good agreement with the microcrack-healing behavior explained for Fig. 9.

4. Conclusions

In this work, the properties of Al_2TiO_5–$MgTi_2O_5$ solid solutions can be summarized as follows:

(1) Except $Al_{2(1-x)}Ti_{1+x}Mg_xO_5$ ($x = 0.0$, i.e. Al_2TiO_5), all samples sintered at 1300–1400°C were composed of single pseudobrookite-type phase. For Al_2TiO_5, a small amount of unreacted Al_2O_3 and TiO_2 were detected.

(2) The increases of grain size and densifications with increasing $MgTi_2O_5$ molar ratio were confirmed. Also thermal expansion increased with increasing $MgTi_2O_5$ ratio.

(3) $Al_{0.2}Ti_{1.9}Mg_{0.9}O_5$ ($x = 0.9$) showed 47.9 MPa as maximum strength. On the other hand, $MgTi_2O_5$ ($x = 1.0$) showed low bending strength (13.2 MPa) despite its high relative density and high CTE.

(4) $Al_{0.6}Ti_{1.7}Mg_{0.7}O_5$ ($x = 0.7$) sintered at 1300°C indicated the highest conductivity. The conductivity of pseudobrookite-type ceramics strongly depend on microcracks.

Acknowledgements This work was supported by Grant-in-Aid for Science Research No. 23350111 for Basic Research: Category B and partly supported by the Sasakawa Scientific Research Grant from The Japan Science Society (Research No. 26-338).

References

1) B. Morosin and R. W. Lynch, *Acta Cryst. B*, 28, 1040–1046 (1972).
2) E. K. Weise and I. A. Lesk, *J. Chem. Phys.*, 21, 801–806 (1953).
3) Y. Ohya and Z. Nakagawa, *J. Mater. Sci.*, 31, 1555–1559 (1996).
4) G. Bayer, *J. Less-Common Met.*, 24, 129–138 (1971).
5) A. Nemoto, K. Iwasaki, O. Yamanishi, K. Tsuchimoto, K. Uoe, T. Toma and H. Yoshino, *Sumitomo Chem. R&D Rep. (International Edition)*, 2011, 1–11 (2011).
6) I. J. Kim, *J. Ceram. Proc. Res.*, 11, 411–418 (2010).
7) V. Buscaglia, G. Battilana, M. Leoni and P. Nanni, *J. Mater. Sci.*, 31, 5009–5016 (1996).
8) G. Tilloca, *J. Mater. Sci.*, 26, 2809–2814 (1991).
9) I. J. Kim and H. Supkwak, *Can. Metall. Quart.*, 39, 387–396 (2000).
10) M. Dondi, *J. Am. Ceram. Soc.*, 92, 1972–1980 (2009).
11) I. J. Kim and L. G. Gauckler, *J. Ceram. Sci. Tech.*, 3, 49–60 (2012).
12) Y. Suzuki and Y. Shinoda, *Sci. Tech. Adv. Mater.*, 12, 034301 (2011).
13) E. A. Bush and F. A. Hummel, *J. Am. Ceram. Soc.*, 41, 189–195 (1958).
14) J. A. Kuszyk and R. C. Bradt, *J. Am. Ceram. Soc.*, 56, 420–423 (1973).
15) K. Daimon, *J. Ceram. Soc. Japan*, 98, 365–369 (1990).
16) Y. Suzuki and M. Morimoto, *J. Ceram. Soc. Japan*, 118, 819–822 (2010).
17) Y. Suzuki and M. Morimoto, *J. Ceram. Soc. Japan*, 118, 1212–1216 (2010).
18) Y. Suzuki, T. S. Suzuki, Y. Shinoda and K. Yoshida, *Adv. Eng. Mater.*, 14, 1134–1138 (2012).
19) B. A. Wechsler and A. Navrotsky, *J. Solid State Chem.*, 55, 165–180 (1984).
20) V. Buscaglia, F. Caracciolo, M. Leoni, P. Nanni, M. Viviani and J. Lemaitre, *J. Mater. Sci.*, 32, 6525–6531 (1997).
21) L. Giordano, M. Viviani, C. Bottino, M. T. Buscaglia, V. Buscaglia and P. Nanni, *J. Eur. Ceram. Soc.*, 22, 1811–1822 (2002).
22) V. Somani and S. J. Kalita, *J. Am. Ceram. Soc.*, 90, 2372–2378 (2007).
23) H. Shin, H.-K. Shin, H. S. Jung, S.-Y. Cho and K. S. Hong, *Mater. Res. Bull.*, 40, 2021–2028 (2005).
24) S. Jayanthi and T. R. N. Kutty, *Mater. Lett.*, 62, 556–560 (2008).
25) C. Sudheendra and T. S. Rao, *Int. J. Sci. Eng. Res.*, 2, 316–319 (2011).
26) P. N. Kapoor, S. Uma, S. Rodriguez and K. J. Klabunde, *J. Mol. Catal. A: Chem.*, 229, 145–150 (2005).
27) Y. Qu, W. Zhou, Y. Xie, L. Jiang, J. Wang, G. Tian, Z. Ren, C. Tian and H. Fu, *Chem. Commun.*, 49, 8510–8512 (2013).
28) H.-J. Steiner, P. H. Middleton and B. C. H. Steele, *J. Alloys Compd.*, 190, 279–285 (1993).
29) C. Zheng, S. Wang, F. Liao, S. Tial and G. Li, *J. Alloys Compd.*, 289, 257–259 (1999).
30) R. Maki and Y. Suzuki, *J. Ceram. Soc. Japan*, 121, 568–571 (2013).
31) I. J. Kim and L. J. Gauckler, *J. Ceram. Process. Res.*, 9, 240–245 (2008).
32) M. Backhaus-Ricoult, C. Glose, P. Tepesch, B. Wheaton and J. Zimmermann, *Ceram. Eng. Sci. Proc.*, 31, 147–164 (2010).